



Stockholm  
University

# Bachelor Thesis

Degree Project in  
Earth Science 15 hp

## **Detecting past storminess through shifts in grain size and mineral composition of aeolian sediments in peat cores**

Johanna Johansson



Stockholm 2024

Department of Geological Sciences  
Stockholm University  
SE-106 91 Stockholm

# Detecting past storminess through shifts in grain size and mineral composition of aeolian sediments in peat cores

Johanna Johansson



Department of Geological Sciences  
Course name: GE6018 Vetenskaplighet och självständigt arbete  
Name of programme: Bachelor's Programme in Earth Science (15 HE)  
Fall/spring term: Spring term 2024  
Supervisor: Malin Kylander  
Examiner: Richard Gyllencreutz  
Assessor: Richard Gyllencreutz, Sarah Greenwood  
© Johanna Johansson  
Cover: Overview photo of Store Mosse

## Abstract

Severe winter storms can cause substantial socio-economic losses. Several climate projections indicate that storminess, that is *frequency* and *intensity* of storms, will increase with an eastward extension into Europe affecting mainly the western and north-central parts. The uncertainty of these projections increases our need to better understand long-term and short-term trends in storminess and storm tracks. Past storminess can be reconstructed by studying aeolian particles deposited in ombrotrophic peat bogs. Peat bogs are great paleoenvironmental archives since they rely solely on atmospheric processes for input. Store Mosse, the largest bog complex in southern Sweden, provides an excellent opportunity to reconstruct past storminess as it has an abundance of local sediment sources available to supply the peat records. A storm record was reconstructed over the last 5200 years for the Store Mosse Dune North (SMDN) sequence, collected from Store Mosse. A peat profile was created where the bulk density, peat accumulation rate and ash content were included. This profile was used to distinguish between the minerotrophic fen and ombrotrophic bog, the fen initiated 5170 cal BP and became fully ombrotrophic in 3675 cal BP. The bulk density and PAR indicated several shifts between drier and wetter conditions, where higher values are linked to drier conditions. Storm events/periods were identified by combining grain size analysis with changes in mineral composition measured by FTIR-ATR. These were identified through peaks in the coarse ( $>125\ \mu\text{m}$ ) fraction and quartz. The fine ( $<38\ \mu\text{m}$ ) fraction dominates the signal and the main minerals identified were quartz (Cp1), mica (Cp3) and K-feldspar (Cp5). Four storm periods could be identified after comparison, these are dated to 3565-3400, 2190-2170, 2005-1900 and 1480-1460 cal BP. These were then compared to storm periods identified in the Store Mosse Dune South (SMDS) storm record, where three were deemed to be related: 2190-2170 (SMDS: 2150-1920 cal BP), 1480-1425 (SMDS: 1450 cal BP) cal BP. SMDS recorded more storm events than SMDN and the main reason for this is believed to be caused by shifting wind directions that weakened the storm signal. These differences indicate the importance of applying different proxy reconstructions and to analyze different sequences within the same site.

## Keywords

Paleo-storms, storminess, Holocene climate, peat cores, aeolian sediments, Store Mosse, Sweden, grain size distribution, ombrotrophic bogs, mineral proxies, NAO

# Contents

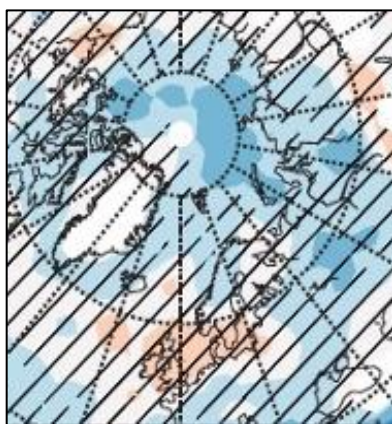
<b>1</b>	<b>Introduction</b>	<b>1</b>
1.1	Storminess	1
1.2	Ombrotrophic peatlands as proxy records	2
1.3	Peatland development	2
1.4	Thesis aims	3
<b>2</b>	<b>Method</b>	<b>4</b>
2.1	Regional setting	4
2.2	Sampling	5
2.3	Chronology and Peat Accumulation Rates	5
2.4	Ash content	6
2.5	FTIR-ATR analysis	6
2.6	Grain size analysis	7
<b>3</b>	<b>Results</b>	<b>7</b>
3.1	Age-depth profile	7
3.2	Peat profile	8
3.3	Grain size profile	10
3.4	Changes in mineral composition	11
<b>4</b>	<b>Discussion</b>	<b>13</b>
4.1	Development of peat deposition and climatic variations	13
4.2	Minerogenic sources	14
4.3	Detecting past storm periods through shifts in grain size	15
4.4	Comparing shifts in grain size and mineral composition	16
4.5	SMDN storm record compared to SMDS storm record	17
4.6	Conclusions	19
	<b>Acknowledgement</b>	<b>20</b>
	<b>References</b>	<b>21</b>
	<b>Appendix</b>	<b>0</b>
	Appendix A: Pre-treated mineral content from Cores 1 and 6	0

# 1 Introduction

## 1.1 Storminess

Severe winter storms have been known to have substantial socio-economic impacts in both marine and terrestrial environments (Orme, 2014). They can cause extreme winds and flooding which damages infrastructure, houses, buildings as well as livelihood. Coastal areas are more vulnerable to storm damage due to both the higher intensity and due to the ongoing sea-level rise. The damage they cause on facilities and physical assets have some years added up to billions of dollars in insured losses (Schwierz *et al.*, 2010). Just in 1990 alone, the total insured losses worldwide amounted to about 14 billion USD. European winter storms exhibit greater annual variability in insured windstorm losses when compared to those worldwide.

There is no clear definition of what constitutes a severe winter storm but they are generally defined as a low probability meteorological event (Nielsen *et al.*, 2024). Storms are defined in terms of wind speed where for example, SMHI defines a storm as having average wind speeds  $>24,5 \text{ m s}^{-1}$  (SMHI, 2023). Many of the most intense winter storms in Europe are formed as extratropical cyclones (ETCs), these are strongly related to the phases of the North Atlantic Oscillation (NAO) (Orme, 2014; Lachance, 2022; Bannister *et al.*, 2024). The imbalance in solar radiation between different latitudes cause pressure differences where large-scale air masses are redistributed from areas of higher pressure to areas of lower pressure. The NAO, which is the dominant mode of variability in atmospheric circulation in the North Atlantic, describes the variability of the atmospheric pressure differences between the Azores high and the Icelandic low. Storminess, that is the *frequency* and *intensity* of storms, increases in wintertime due to the greater pole-equator temperature gradient with poleward energy transport.



Number density per unit area per month  
*Fewer storms* *More storms*

**Fig. 1.** Projected winter storm track density for 2080-2100 under SSP5-8.5 based on 13 CMIP6 models. Hatching is where 80% of models do not agree on the sign of the change (IPCC, 2021).

Storminess is expected to increase over many parts of Europe including Scandinavia (Orme, 2014; IPCC, 2021). Several climate projections indicate that the changes will be uneven due to anthropogenic climate change (Schwierz *et al.*, 2010; Severino *et al.*, 2024). The increase is predicted to occur with an eastward extension affecting both the western and north-central parts and to decrease over the rest of Europe (figure 1). For all these projections it is emphasized that there is a high uncertainty, especially for regions where storminess is expected to increase, this is largely due to a lack of high resolution long-term data (Lachance, 2022). However, these uncertainties make it even more important to increase our knowledge of both storminess and storm tracks and to better understand its relation to the NAO variability. To achieve this both long-term and short-term trends are necessary, not only in coastal areas but also inland. Better predictions

would give authorities, insurers and industries the chance to prepare more effectively (Orme, 2014).

## 1.2 Ombrotrophic peatlands as proxy records

There are several different proxy-based methods for reconstructing Holocene storminess. One of these involves studying aeolian particles deposited in ombrotrophic peat bogs (de Jong, 2007; Orme, 2014). Ombrotrophic bogs receive their input solely from atmospheric processes and the anoxic conditions preserve the organic remains and so also the mineral deposits. Peat has several advantages as paleoenvironmental archives. Consisting mostly of partially decayed organic material, it is easy to date (de Jong, 2007; Lachance, Peros and St-Jacques, 2022), but most importantly; it accumulates continuously. It is able to quickly trap the deposited sediments and provide long, continuous records with high resolution.

The paleo-storm method in peats is based on the concept that more and coarser clastic sediments are transported during periods of high wind conditions. This was first introduced by Björck and Clemmensen (2004) where they used the fluctuations of aeolian sand influx (ASI) which measures variations in grains between 200-350  $\mu\text{m}$  and  $>350 \mu\text{m}$ . The inverse of the loss-on-ignition (LOI) procedure was also used to provide an estimate of the mineral content of the peat. Since this work, several other proxies have since been developed that are beyond the traditional sedimentological approach such as the LOI and grain size measurements. For example, there is also the inorganic geochemical approach such as elemental chemistry (Sjöström *et al.*, 2022) and X-ray diffraction (XRD) that identifies and quantifies the mineral content as some are linked to coarser grain sizes, such as quartz and K-feldspar (Kylander *et al.*, 2023; Yao *et al.*, 2023). A relatively new approach, that also establishes the mineralogy of the archived material, is the Attenuated total reflectance Fourier-transform infrared spectroscopy (FTIR-ATR) analysis (Martínez-Cortizas *et al.*, 2021). With this there is no need for sample preparation as it is quick and non-destructive to use. One disadvantage of this type of paleo-storm reconstructions however, is that for this to work there has to have been an abundance of sediment sources available containing various grain sizes located closely to the bog.

Research utilizing the mineral content in peatlands as proxies has mostly been conducted in Northern Europe (Chambers *et al.*, 2012) but there have also been similar studies conducted in for example, China, Indonesia and Canada. In Sweden, where the very first paleo-storm records come from, we have a number of records. These have been synthesized in a recent article by (Kylander *et al.*, 2023). They compared the paleo-storm records, all located within southern Sweden, to each other and to their own reconstruction of inland past storminess for the Store Mosse Dune South (SMDS) sequence collected from Store Mosse (in Swedish “the Great Bog”) (figure 2). The aim was to better understand past storminess over wider geographical areas and changes in storm track movements over time.

## 1.3 Peatland development

Peat is formed in situ in mires which commonly in Sweden grades between nutrient-rich minerotrophic fens and nutrient-poor ombrotrophic bogs (Rydin and Jeglum, 2013b). Bogs are strongly acidic (pH of 4-5) with a low degree of humification. They grow above the groundwater table either on top of fens or wet forests and are mainly dominated by different *Sphagnum* mosses. Bogs and fens mostly form in moist conditions, with annual temperatures between  $-12^{\circ}\text{C}$  to  $+6^{\circ}\text{C}$  and an annual precipitation between 200-1000 mm (Sohlenius *et al.*, 2013). There are three main formation processes: terrestrialization, paludification and primary peat formation (Rydin and Jeglum, 2013a). Terrestrialization is when a shallow pond or lake is filled from its margins with sediment and peat. Paludification refers to peatlands formed on

top of drier soil surfaces with previous vegetated conditions, the peat is often woody at the base of these profiles. Primary peat formation refers to peatlands accumulating directly on top of mineral soils with no previous open body of water or vegetation.

The rate at which peat accumulates is controlled by the production rate of new litter and the decomposition rate, with the latter being the most important factor (Belyea and Malmer, 2004; Sohlenius *et al.*, 2013). These rates are influenced by several different factors such as climatic conditions, local vegetation, nutrient status, hydrology and the position of the water table. Wetter conditions with a low evapotranspiration with intermediate temperatures (0-2.5°C) generally generate higher accumulation rates. The average rate of primary production and decomposition are usually low in mires. Both of these rates are relatively high in the uppermost part, the acrotelm, located within the aerobic zone and above the mean water table. Below this in the catotelm, the anaerobic zone, the decay rate slows down drastically thus preserving the litter. The mean water table is positioned between these two layers which makes the catotelm permanently saturated while the acrotelm is saturated periodically (Franzén, 2006).

Accumulation rates are usually higher in bogs than in fens. *Sphagnum* species have a low rate of decomposition and a low rate of primary production (Sohlenius *et al.*, 2013). The accumulation rate is higher because of their high resistance to decomposition and the anoxic, saturated, nutrient-poor and acidic conditions that inhibits microbiological activity. The production for a fen is usually greatest in the beginning of its development, as it grows upwards it becomes more isolated from the ground waters and primary production rate reduces while decomposition rate increases.

Another important difference between bogs and fens is that bogs are shut off from the groundwater. As such all nutrient input comes from the atmosphere and these are therefore very nutrient poor systems. This however, also means that peat bogs present an atmospheric record.

## 1.4 Thesis aims

Reconstructing past storms and understanding their relation to climate variations is important in order to enhance our chances of predicting future changes in storminess. This project aims to reconstruct inland storminess over the last 5200 years by analyzing the clastic sediments deposited in a peat bog sequence from an ombrotrophic bog. The study will be conducted using ash content, grain size analysis and FTIR-ATR inferred mineralogy. This will be built on Vikdahl's (2021) earlier work on the Store Mosse Dune North (SMDN) sequence from Store Mosse mire located in south-central Sweden (figure 2). Only his elemental work will be utilized, this report will augment it with more analyses and also with grain size and mineralogical data. Several other sequences have been analyzed from this mire before (Kylander *et al.*, 2023). The previously mentioned SMDS is one of them and is located close to the SMDN sequence (ca. 2 km southwest) with a bisecting dune separating them, providing an excellent opportunity for comparison within a site.

The aims for this thesis are to:

1. Create and analyze a peat profile of the SMDN sequence and link it to past climatic conditions
2. Measure the fluctuations in the grain size distribution and median diameter in the SMDN sequence.
3. Measure the variations in mineral composition through the SMDN profile.
4. Construct a storm record in the SMDN sequence based on point 1-3.
5. Compare the storm records from SMDN and SMDS.

## 2 Method

### 2.1 Regional setting

Store Mosse (57°15'N, 13°55'E, figure 2), situated at 160-170 m a.s.l., is the largest bog complex in southern Sweden (Svensson, 1988; Belyea and Malmer, 2004). The ice sheet began its retreat ca. 15-16 ka in southern Sweden (Persson, 2008). The melting water formed large areas with rivers and lakes of ice along with deposits of sand and moraine. Store Mosse deglaciated ca. 14 ka (Lundqvist and Wohlfarth, 2001) and was instead covered by the postglacial ice-dammed lake Fornbolmen. This lake was later gradually drained as it was tipped to the south due to the uneven isostatic uplift. The sand at the bottom of the lake was reworked by the wind several times and formed a net of dune ridges, also known as rocknar (Sveriges Nationalparker, 2024), and islands. *Carex* fen began to form 8-9 ka in this sandy and oxygen-poor environment due to the climate growing milder and more humid (Ryberg *et al.*, 2022). The climate continued to grow colder with a reduction of the water levels ca. 5 ka that caused the transition from minerotrophic fen to ombrotrophic bog.

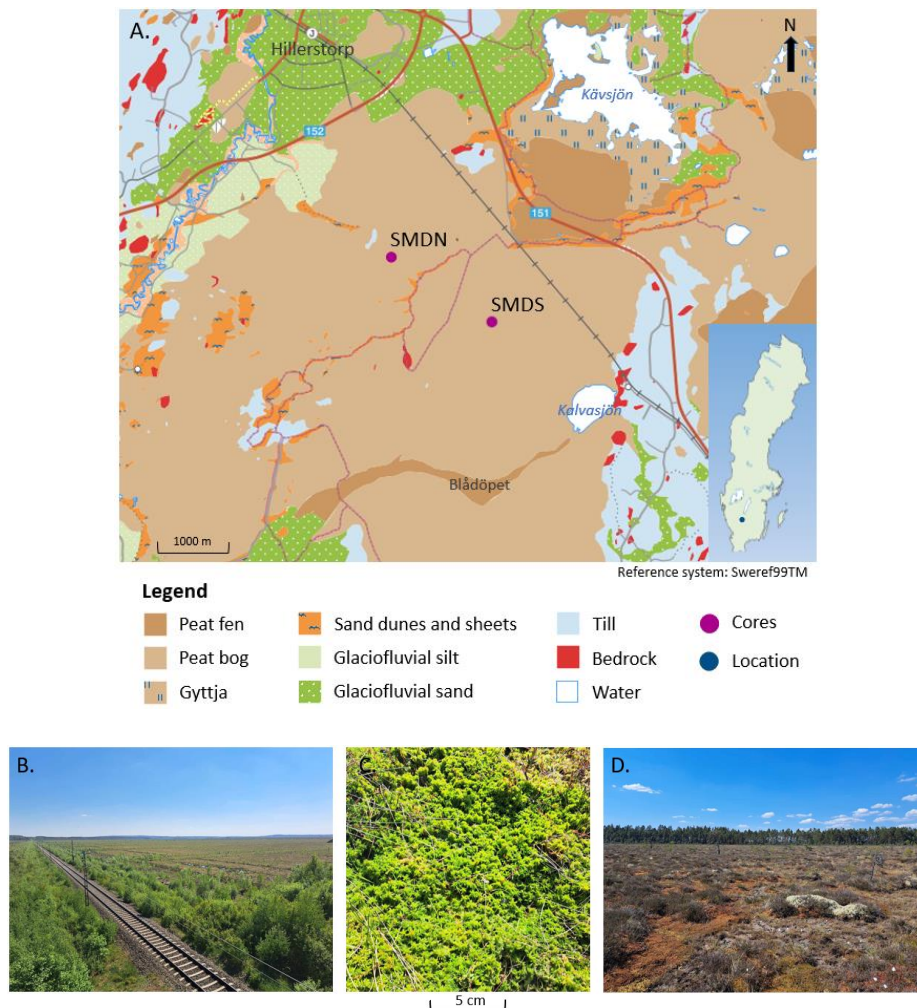


Figure 2. A. Soil map of Store Mosse national park with the locations of the SMDN and SMDS. Both the soil map and the inset are edited screenshots from “Jordartskartan 1:25 000 – 1:100 000” shown in kartvisaren ©Geological survey of Sweden (SGU, 2018). B. Photo of the remains of the train tracks crossing the mire and some of the drainage ditches. C. Close up photo of *Sphagnum* moss before being

dried. D. A representative overview photo of the SMDS bog in Store Mosse, the pine trees in the background grow on dune ridges separating the bogs from each other.

The mire is presently made up of three main larger bog areas centered around lake Kävsjön, and a number of smaller fens that drain the bogs with several bisecting sand dunes (Svensson, 1988; Kylander *et al.*, 2023). The bogs are largely made up of various *Sphagnum* mosses and the mire has a thickness that can reach over 5 m in the west-central areas. The bedrock consists mainly of grey and red-grey gneisses and granite (Hansson, 2013). Hourly measurements between 2013-2023 from the closest weather station, Hagshult, gives an average annual precipitation of 734,5 mm yr<sup>-1</sup> (SMHI, 2024b) and an average annual temperature of 6.8°C (SMHI, 2024a). The amount of days where the mean temperature is above 4°C, the growing season, is about 210 days (Belyea and Malmer, 2004). More than 0,1 km<sup>2</sup> of the bog was subjected to drainage and peat cutting between 1905-1966 (Adamsson, 2013; van Ravenhorst, 2022). The drainage ditches are still visible around the rail road, used to transport the peat, crossing the mire and dividing it into two parts.

The SMDN (57°17'7.69"N, 13°54'8.79"E) and SMDS (57°16'37.70"N, 13°55'30.86"E) sequences (figure 1) are in some of the largest bogs of the area and are located just south of lake Kävsjön (Kylander *et al.*, 2023). They both belong to a deeper part of the mire with various *Sphagnum* mosses dominating. The surrounding sand sheets and glaciofluvial sediments act as local sources of sediments along with bisecting ridges of sand dunes separating the bogs from each other.

## 2.2 Sampling

The lobe southwest of the dune system at Store Mosse was sampled in September 2017 and named the SMDN sequence (Vikdahl, 2021). Cores were taken with a 1 m long Russian corer with a diameter of 7.5 cm. The samples were collected by alternating between two adjacent parallel holes. Six 1 m long sections were obtained with a 25 cm overlap for each core.

The cores were subsampled, after being stored under cold conditions, into 2 cm thick slices (Vikdahl, 2021). All sections were stored in zip-lock bags labeled with their section number; every section also had an additional bag containing cut out peat with a volume of 1 cm<sup>3</sup>. The samples were then frozen for 24 hours and put into a freeze-drier for at least four hours to dehydrate them.

## 2.3 Chronology and Peat Accumulation Rates

The age-depth model was constructed by Jenny Sjöström (Vikdahl, 2021). The chronology of the sequence is based on radiocarbon dating of plant macrofossils. The chronology was based on two <sup>14</sup>C dates that were calibrated to calendar years and the composite depth of the sequence. The age-depth model was plotted in the R Bacon software using the the IntCal20 <sup>14</sup>C calibration curve (Reimer *et al.*, 2020).

The dry bulk density was measured and used to align the cores and obtain the composite depth of 508 cm. The values for the dry bulk density were given by (Vikdahl, 2021). It was calculated for one sub-sample in each section by measuring and dividing their dry weights with their volumes.

The bulk density and the age-depth model were used to calculate the peat accumulation rate (PAR) in excel with equation:

$$PAR_i = \frac{BD_i * d}{t_{i+1} - t_i} \quad (1)$$

Where BD= bulk density, d= thickness of the sample (2 cm), t= years BP and i= 1, 2, 3....

## 2.4 Ash content

The LOI procedure was used to determine the ash content of the samples. Here we present this as the ash content (i.e., 100%-LOI). Two adjacent sub-samples were selected in the top 4 cm of 10 cm intervals in each core, a total of 88 samples were collected. Empty crucibles were numbered and left to dry in an oven for at least four hours at 105°C to remove any water. These were then weighed after cooling in a desiccator for 30 minutes. The sub-samples were added to the crucibles and then dried again at 105°C for at least 4 hours. The crucibles were then weighed again after cooling in a desiccator for 30 minutes to determine the organic dry weight. They were then combusted in a high temperature oven at 550°C for 7 hours to obtain the ignition residue. The samples were kept at a temperature of 105°C and weighed after cooling in a desiccator for 30 minutes. The minerogenic content was calculated relative to the organic content with equation:

$$Ac_i = \frac{Wa_i - Wc_i}{Wd_i - Wc_i} * 100 \quad (2)$$

Where Ac= ash content, Wa= the dry weight of the ash, Wc= the dry weight of the crucible, Wd= the dry weight of the sample and i= 1, 2, 3...

The mineral matter was then put in several different glass jars with their corresponding section number written on them.

## 2.5 FTIR-ATR analysis

The ashed samples were analyzed by Thermo Scientific Nicolet iS5 FT-IR equipped with an iD7 Diamond ATR. Measurements were recorded with a wavelength range of 4000-400 cm<sup>-1</sup> at a resolution of 4 cm<sup>-1</sup> and by averaging 100 scans for each sample.

A small fraction of the ashed peat was placed on the ATR crystal with a lab spoon. The ash was then compressed three times into the substrate surface. For each sample a background spectra was collected before the sample was measured. The data spacing was changed to 2.0 to conform to the requirements of the using {andurinha} R package (Fernandez and Cortizas, 2020) which was used to process the data. The sample was then transferred back to its glass jar by putting it on some tin foil with the lab spoon. The labware and the diamond window were cleaned with ethanol and Kleenex tissues before and after use. During use only the labware was cleaned with ethanol between each sample. The crystal surface was instead cleaned with tissues and compressed air to not let the ethanol affect the results.

The data was saved as CSV files and sent to Antonio Martínez-Cortizas, Professor of Soil Science at the University of Santiago de Compostela, for statistical analysis following his recent publication (Martínez-Cortizas *et al.*, 2021). Shortly, the data are treated using principal component analysis and the extracted components are then compared to reference spectra for major minerals (quartz, microcline, orthoclase, albite, anorthite, muscovite, biotite, calcite, amphibole) obtained from the RRUFF

database (<http://rruff.geo.arizona.edu>). In this work only the profiles for mica, anorthite, quartz and K-feldspar are considered due to their relevance to the question and following (Kylander *et al.*, 2023).

## 2.6 Grain size analysis

The samples were pre-treated before measuring their grain size distribution to remove calcite and any residue organic material. The peat ash was first dissolved in 10% hydrochloric acid (HCl) solution for 2 hours while placed in a fume hood. They were then transferred to 50 ml centrifuge tubes, each labeled with their corresponding section number. A squeeze bottle with deionized water was used to wash down any residue. The tubes were vortexed in an ultrasonic cleaner for 30 seconds for de-clumping and then diluted with deionized water to a total volume of 45 ml. They were centrifuged at 4000 rpm for 10 minutes and then reduced to a total volume of 10 ml. The samples were vortexed, diluted, centrifuged and reduced two more times but instead with a vortex time of 10 seconds in a vortex mixer.

The particle size distributions of the washed samples were determined with a Malvern 3000 laser diffraction particle size analyzer with a particle size range from 0,0100-3500  $\mu\text{m}$ . The stirrer was set to 3500 rpm, the sample measurement duration to 30 seconds and the obscuration range to 2-15%. A dispersing agent solution consisting of 6 ml of 10% sodium metaphosphate ( $\text{NaPO}_3$ ) solution was added with a pipette before every background measurement. Then 10-20 ml was removed with another pipette. Each sample was vortexed and left for three minutes in the analyzer before measurement. An adjacent sample was added whenever the obscuration range was below 2%. Five measurements were run in a row for every sample. The relative standard deviation (RSD) of these five measurements had to be less than 5%. The measurements were stopped and re-initialized where the RSD was above 5 %, this was repeated until five full measurements had an RSD below 5%.

The files were converted to excel-files and average values were calculated from the five measurements of each sample. The data was divided into different size fractions those presented in this report are fine %(<38  $\mu\text{m}$ ), medium %(38-63  $\mu\text{m}$ ), medium coarse %(63-125  $\mu\text{m}$ ), coarse %(>125  $\mu\text{m}$ ) and the median diameter  $\mu\text{m}(\text{Dx}(50))$ .

## 3 Results

### 3.1 Age-depth profile

The age-depth model (figure 2), generated by Jenny Sjöström, consists of two linear segments based on two calibrated  $^{14}\text{C}$  dates. The ages are presented as calendar years before present (cal BP). The first calibrated age was dated to 2828 cal BP at a depth of 324 cm and the second calibrated age was dated to 5169 cal BP at a depth of 490 cm. Two linear weighted means were calculated from this with a 95% confidence interval. Given the uncertainty of the age-depth model all ages have been rounded up to the nearest 5 years.

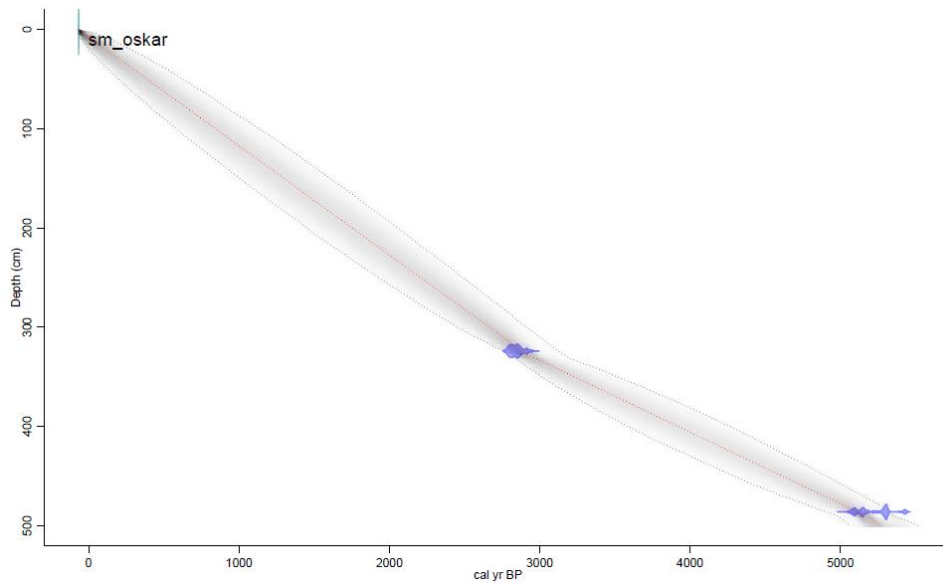


Figure 3. Age-depth model of the SMDN sequence. The red dotted line represents the linear weighted means for the two calibrated  $^{14}\text{C}$  dates. The gray scale represents the 95% confidence range. The ages are given in calendar years before present (cal BP).

### 3.2 Peat profile

The properties of the peat regarding bulk density, PAR and ash content were combined with the age-depth model from figure 2 to produce a vertical profile of the SMDN sequence ranging from 390 to 5170 cal BP (figure 3). The peat sequence starts at 390 cal BP because the top 50 cm of the sequence was not collected during sampling. The average values are given as means and standard deviations ( $1\sigma$ )

The bulk density of the SMDN sequence ranges from  $0,04$  to  $0,30\text{ g cm}^{-3}$  ( $n=219$ ) with an average value of  $0,12 \pm 0,06\text{ g cm}^{-3}$ . The bulk density of the fen section ranges from  $0,14$  to  $0,30\text{ g cm}^{-3}$  with an average value of  $0,20 \pm 0,04\text{ g cm}^{-3}$  while the bog section ranges from  $0,04$  to  $0,22\text{ g cm}^{-3}$  with an average value of  $0,09 \pm 0,04\text{ g cm}^{-3}$ . The bulk density has its maximum value of  $0,30\text{ g cm}^{-3}$  at the base and generally decreases to  $0,15\text{ g cm}^{-3}$  in 4390 cal BP. This is followed by a rapid increase to  $0,25\text{ g cm}^{-3}$  at 4310 cal BP where it displays a decreasing trend again until 3840 cal BP ( $0,23\text{ g cm}^{-3}$ ). From here two rapid decreases after each are observed, the first ends at  $0,13\text{ g cm}^{-3}$  in the fen-bog transition at 3675 cal BP while the second ends at  $0,08\text{ g cm}^{-3}$  at 3370 cal BP. This is followed by a relatively stable periods with small fluctuations and bulk densities below  $0,1\text{ g cm}^{-3}$ . Two sharp increases are observed from 2520 to 1570 cal BP with a maximum value of  $0,22\text{ g cm}^{-3}$  in 2025 cal BP. After a decrease to  $0,07\text{ g cm}^{-3}$  from 1735 to 1570 cal BP it becomes relatively stable again until 390 cal BP.

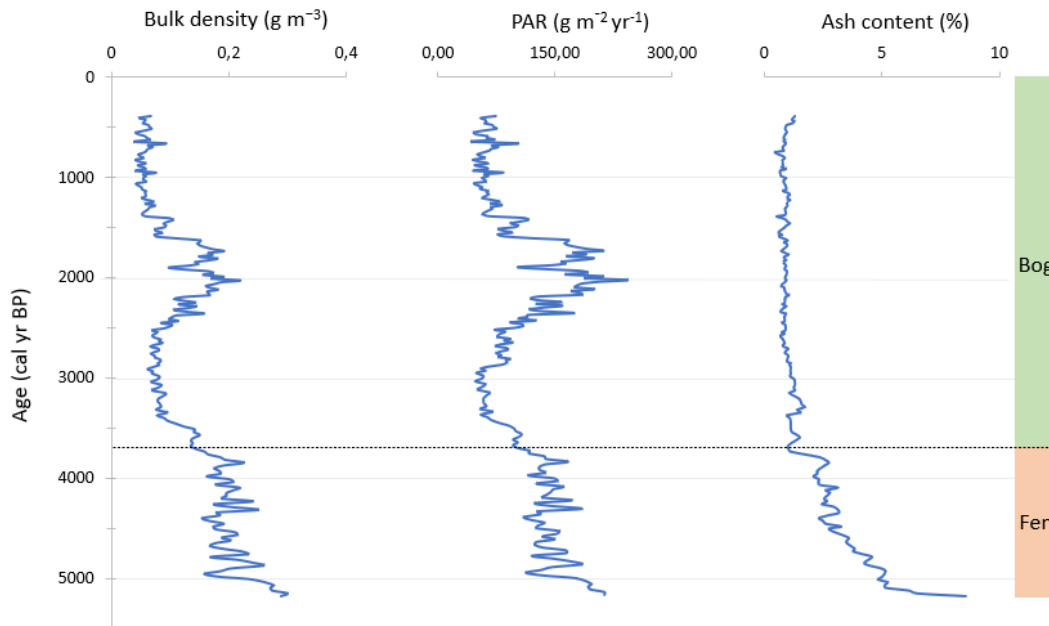


Figure 4. The bulk density ( $\text{g cm}^{-3}$ ), the PAR ( $\text{g m}^{-2} \text{yr}^{-1}$ ) and the ash content (%) from 5170 to 390 cal BP of the SMDN sequence. The dotted line at 3675 cal BP, is when the fen is interpreted to have transitioned fully into an ombrotrophic bog.

The PAR of the SMDN sequence ranges from 43 to 243  $\text{g m}^{-2} \text{yr}^{-1}$  ( $n=219$ ) with an average value of  $109 \pm 47 \text{ g m}^{-2} \text{yr}^{-1}$ . The PAR in the fen section ranges from 102 to 214  $\text{g m}^{-2} \text{yr}^{-1}$  with an average value of  $146 \pm 26 \text{ g m}^{-2} \text{yr}^{-1}$  while the PAR in the bog section ranges from 43 to 243  $\text{g m}^{-2} \text{yr}^{-1}$  with an average value of  $97 \pm 47 \text{ g m}^{-2} \text{yr}^{-1}$ . The PAR generally corresponds well to the bulk density curve since the two weighted means in the age-depth model are linear (see figure 2 and equation 1). It decreases to 110  $\text{g m}^{-2} \text{yr}^{-1}$  from the base to 4390 cal BP. It increases slightly to 184  $\text{g m}^{-2} \text{yr}^{-1}$  at 4310 cal BP to then decrease slowly to 167  $\text{g m}^{-2} \text{yr}^{-1}$  at 3840 cal BP. Then there are two rapid decreases after each other, the first decrease is to 96  $\text{g m}^{-2} \text{yr}^{-1}$ , right after the fen-bog transition at 3675 cal BP, and the second decrease is to 55  $\text{g m}^{-2} \text{yr}^{-1}$  at 3370 cal BP. It stays relatively stable with PAR values below 100  $\text{g m}^{-2} \text{yr}^{-1}$  until 2520 cal BP however, there is a positive shift for the rest of the PAR after 2910 cal BP that isn't displayed for the bulk density curve. Two phases of rapid increases can be observed from 2520 to 1570 cal BP where the PAR has its maximum value of 243  $\text{g m}^{-2} \text{yr}^{-1}$  at 2025 cal BP. After a rapid decrease from 1735 to 1570 cal BP it becomes relatively stable again with small fluctuations until 390 cal BP.

All cores possess a low mineral content, especially in the bog section. The ash content of the SMDN sequence ranges from 0,5 to 8,6 % ( $n= 200$ ) with an average value of  $1,6 \pm 1,3$  %. The ash content in the fen ranges from 1,0 to 8,6 % with an average value of  $3,5 \pm 1,5$  % while the ash content in the bog ranges from 0,5 to 1,7 % with an average value of  $1,0 \pm 0,2$  %. The ash content has its maximum value at the base (8,6 %). There is a rapid decrease to 5,2 % at 5085 cal BP followed by an overall slow decrease. There is a slight increase from 3980 to 3840 cal BP. From there another rapid decrease is observed to 1,0 % in the fen-bog transition at 3675 cal BP. The ash content stays below 2 % through the whole bog section and is relatively stable from the transition to 390 cal BP with small fluctuations.

### 3.3 Grain size profile

Two different grain size profiles of the SMDN sequence are shown in figure 4, presenting the fluctuations of the grain size distribution of the coarsest fractions and the median diameter. The sediments were divided into four different size fractions: coarse ( $>125\ \mu\text{m}$ ), medium coarse ( $63\text{-}125\ \mu\text{m}$ ), medium ( $38\text{-}63\ \mu\text{m}$ ) and fine ( $<38\ \mu\text{m}$ ). Since the fine fraction dominates the signal ( $>90\%$  on average) it is not presented in the figure but rather makes up the remainder of the material through the profile. There is no data from the base to 4335 cal BP because the excessive amount of unknown material in core 6 (see appendix A) was too much for the analyzer to run in one measurement. Obtaining a representative distribution for this core was therefore difficult. The average values are given as means and standard deviations ( $1\ \sigma$ ). Most samples were measured together with their adjacent sample in the analyzer due to low obscuration values, these are given as time periods.

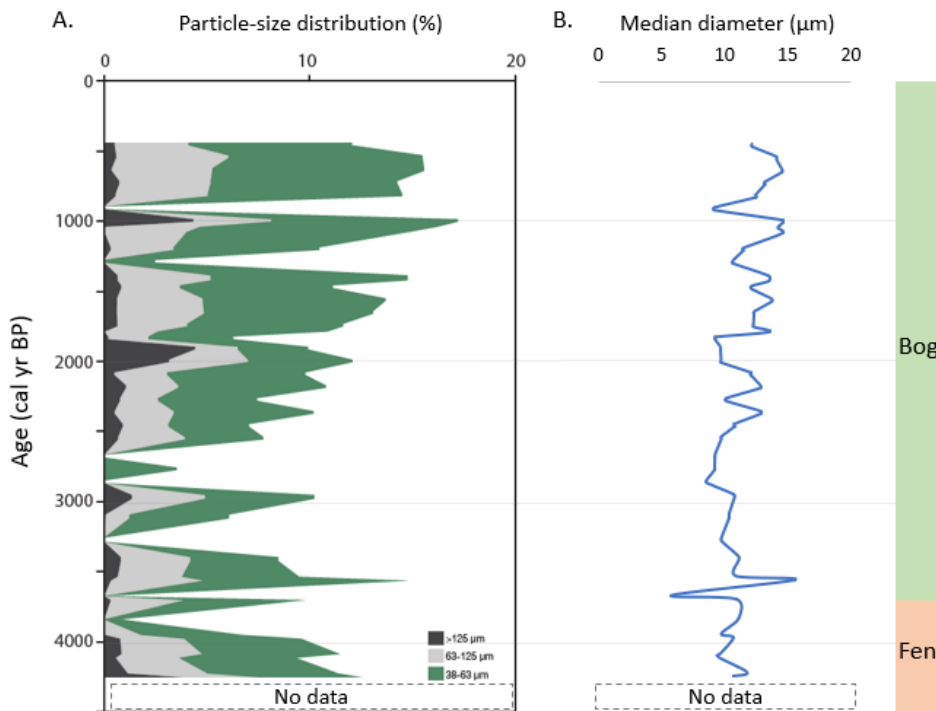


Figure 5. Two graphs of the particle-size distribution and the median diameter for the minerogenic material from 4255 to 445 cal BP and the fen and bog division. There is no data from the base to 4255 cal BP. A. The grain size distribution is expressed as percentages and are divided into three size fractions: coarse ( $>125\ \mu\text{m}$ ), medium coarse ( $63\text{-}125\ \mu\text{m}$ ) and medium ( $38\text{-}63\ \mu\text{m}$ ). The fine ( $<38\ \mu\text{m}$ ) fraction is not presented in the figure but makes up the remainder of the material through the profile. B. Shows the variations of the median diameter through the profile.

There are several shifts in the grain size distribution for all size fractions. The fine ( $<38\ \mu\text{m}$ ) fraction is the most abundant through the whole sequence, it ranges from  $82,8$  to  $100\%$  with an average value of  $90 \pm 4,9\%$ . It makes up  $100\%$  of the material five times through the sequence, with the first two occurring at  $3840$  and  $3675$  cal BP. The other four times occur at  $3285\text{-}3260$ ,  $2870\text{-}2850$ ,  $2685\text{-}2670$  and  $915\text{-}890$  cal BP. The other three size fractions show great fluctuations between these occurrences. An increase for the coarse ( $>125\ \mu\text{m}$ ) fraction generally means a decrease for the other two presented size fractions with a few exceptions. The fen section, from  $4255$  to  $3675$  cal BP, has its coarsest grains at the base where the coarse ( $>125\ \mu\text{m}$ ) fraction has a value of  $3,8\%$  and the medium coarse ( $63\text{-}125\ \mu\text{m}$ ) fraction has a value of  $3,7\%$ . The three size fractions decrease rapidly until the fen-bog transition at  $3675$  cal BP.

The coarse (>125 µm) fraction ranges from 0 to 4,4 % with an average value of  $0,8 \pm 1,1$  %. Two peaks are observed from 3675 to 2870 cal BP, these are centered on 3565-3400 (0,8 %) and 2980-2955 (1,4 %) cal BP. It decreases to values around 0 % from 2870 to 2670 cal BP. Great fluctuations are displayed from 2670 to 445 cal BP, all three size fractions have several small peaks centered around two greater peaks for the coarse (>125 µm) and medium coarse (63-125 µm) fractions. Small peaks for the coarse (>125 µm) fraction occur at 2465-2450 (0,9 %) and 2190-2170 (1,1 %) cal BP before its maximum value of 4,4 % between 2005 and 1900 cal BP which is followed by two peaks in 1480-1460 (0,8 %) and 1210-1190 (0,3 %) cal BP. The second large peak occur in 1005-990 cal BP with a value of 4,3 %. Followed by one small peak at 735-715 cal BP with a value of 0,7 %.

The medium coarse (63-125 µm) fraction ranges from 0 to 5,5 % with an average value of  $2,7 \pm 1,6$  %. It fluctuates greatly through the whole sequence. It increases from 0 to 4,5 % from 3675 to 3565 cal BP and displays two peaks in 3425-3400 (3,4 %) and 2980-2955 (3,6 %) cal BP. This is followed by a decrease from 2870 to 2685 cal BP with values around 0 %. The peaks generally increase from 2670 to 445 cal BP with peaks centered on 2560-2540 (3,3 %), 2375-2355 (2,9 %), 2005-1990 (3,8 %), 1660-1550 (4,2 %), 1425-1390 (4,5 %), 1045 (4,6 %) and 550-535 (5,5 %) cal BP.

The medium (38-63 µm) fraction ranges from 0 to 11,5 % with an average value of  $5,8 \pm 3,1$  %. It has an overall decreasing trend in the fen section and presents an overall increasing trend through the bog section. The first peak occurs at 3565 (9,9 %) cal BP and the second in 3120-2955 (5,3 %) cal BP. There is a decrease from 2870 to 2685 cal BP with very low values ranging from 0 to 3,5 %. Two small peaks from 2670 to 1915 cal BP are centered in 2375-2355 (6,8 %) and 2190-2170 (7,2 %) cal BP. It decreases rapidly to 3,4 % in 1915-1890 cal BP where the coarse (>125 µm) fraction has its maximum value. Followed by two peaks in 1425-1390 (9,6 %) cal BP and its maximum value at 1045 (11,5 %) cal BP. It decreases in 1005-990 (9 %) cal BP where the coarse (>125 µm) fraction has a value of 4,3 %. It rapidly decreases until 915-890 cal BP followed by a sharp increase in 645-625 (10,3 %) cal BP where it decreases slightly until 445 cal BP.

The samples had median grain sizes between 5,8 and 15,5 µm with an average value of  $11,3 \pm 1,9$  µm. Its lowest value is observed right after a rapid decrease from 3700 to 3675 cal BP (5,8 µm), with its highest value occurring right after in 3565 cal BP. It is relatively stable until 2685 cal BP where it fluctuates back and forth until 390 cal BP with peaks centered on 2375-2355 (12,8 µm), 2190-2170 (12,8 µm), 1780 (13,5 µm), 1570-1550 (13,7 µm), 1425-1390 (13,5 µm), 1080-990 (14,6 µm) and 645-625 (14,5 µm) cal BP.

### 3.4 Changes in mineral composition

The main minerals identified by FTIR-ATR analysis of the ashed material in the SMDN sequence were quartz, principal component 1 (Cp1), mica (Cp3) and K-feldspar (Cp5). Individual partial communalities are presented in figure 5, they reflect relative changes of each mineral through the sequence. The average values of the identified minerals are given as means and standard deviations ( $1 \sigma$ ).

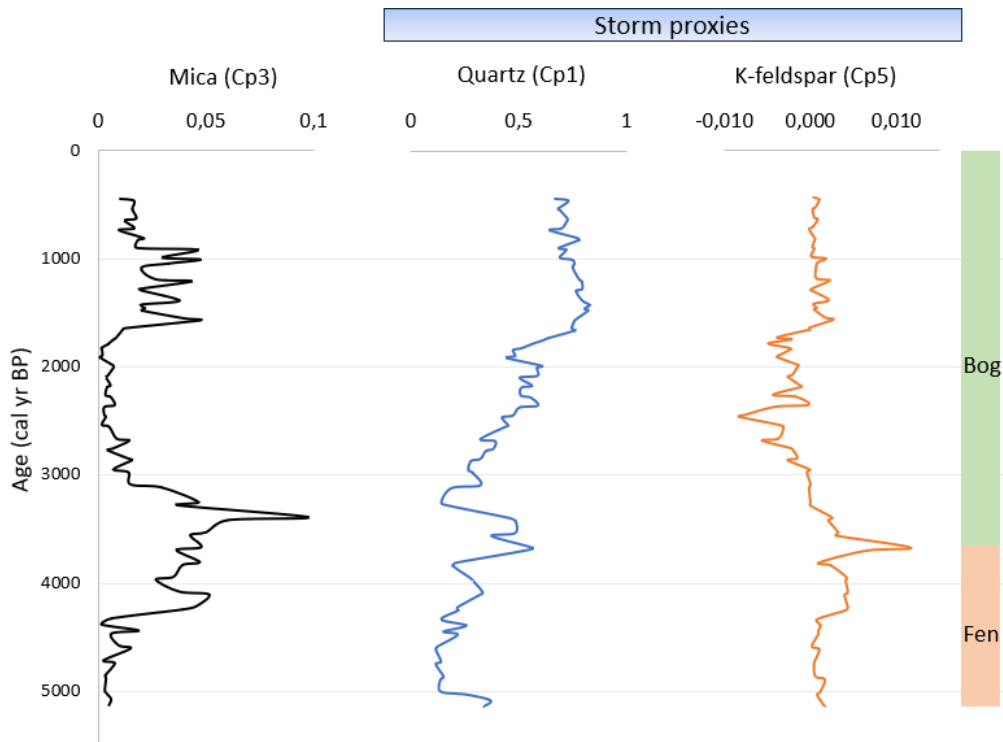


Figure 6. Individual partial communalities of the main minerals identified by FTIR-ATR analysis of the ashed peat samples in the SMDN sequence between 5140 and 445 cal BP, and the fen and bog division. The identified minerals are mica (biotite and muscovite) principal component 3 (Cp3), quartz (Cp1) and K-feldspar (Cp5).

Mica (Cp3), includes both biotite and muscovite and has an average value of  $0,019 \pm 0,018$ . It generally increases from the base to 3400 cal BP, peaks are observed at 4615, 4450, 4115, 3810, 3675 and 3400 cal BP. It decreases until 2560 cal BP with peaks observed at 3260, 2870 and 2690 cal BP. From 1780 to 445 cal BP five peaks are centered on 1570, 1390, 1210, 1005 and 915 cal BP.

The sequence is mainly dominated by quartz (Cp1) with an average of  $0,48 \pm 0,22$ . It presents a generally increasing trend from the base and upwards. The first main increase is observed from 3840 to 3260 cal BP consisting of two peaks, the first peak is in the fen-bog transition at 3675 cal BP and the second peak is between 3535 and 3400 cal BP. There is a gradual increase from 3260 to 1915 cal BP with small fluctuations, small peaks occur at 3095, 2685, 2540, 2355, 2170 and 2080-1990 cal BP. A small decrease is followed by a rapid increase between 1915-1660 cal BP. A small gradual decrease can be seen from 1660 to 445 cal BP with small fluctuations. Followed by small peaks centered at 1480-1425, 825-805, 645 and 460 cal BP.

K-feldspar (Cp5) presents low values through the sequence with an average value of  $0 \pm 0,003$ . A wide peak can be seen from 4335 to 3810 cal BP and is followed by a sharp increase in the fen-bog transition at 3675 cal BP. Values are below zero between 3285 and 1645 cal BP with small increases occurring at 2560, 2355, 2190-2170, 2005-1990, and 1840 cal BP. Small fluctuations are observed from 1645 to 445 cal BP with peaks at 1570, 1390, 1210 and 1005 cal BP.

## 4 Discussion

### 4.1 Development of peat deposition and climatic variations

The fen initiated ca. 5170 cal BP at the SMDN coring site, despite other studies suggesting that fen formation started ca. 9000-8000 cal BP. Kylander *et al.* (2023) conducted a ground-penetrating radar (GPR) survey of the area with profiles showing that the peat depth varies greatly across the mire, indicating the existence of numerous sub-basins. Their interpretation was that the oldest peat sequences are located in the southern parts of the bog complex and only after the dune emplacement ca. 8000-6000 cal BP (Bjermo, 2019) could the areas north of Blådöpet begin to accumulate peat (figure 2).

Woody fragments were observed in Cores 5 and 6 (5170-3370 cal BP) which indicate peatland formation through paludification on the underlying layers of sand. Both Svensson (1988) and Ryberg *et al.* (2022) agree with this and note that paludification is a common peatland formation process in south-western Sweden. It is also mentioned that in the southern parts fen initiation occurred through terrestrialization, as an oligotrophic lake remained there after the drainage of the Fornbolmen ice lake. The fen initiation here was due to a wetter and warmer climate from 8145 to 7000 cal BP that then became drier and less humid (Ryberg *et al.*, 2022). The climate gradually shifted toward dry and cool conditions around 6500-5900 cal BP which lasted until ca. 4500 cal BP. The dry conditions increased peat accumulation in the area and initiated the fen development at the SMDN coring site.

The average bulk density and the PAR are higher in the fen section ( $0,20 \pm 0,04 \text{ g cm}^{-3}$ ,  $146 \pm 26 \text{ g m}^{-2} \text{ yr}^{-1}$ ) than the bog section ( $0,09 \pm 0,04 \text{ g cm}^{-3}$ ,  $97 \pm 47 \text{ g m}^{-2} \text{ yr}^{-1}$ ) (figure 4). The top 50 cm wasn't collected during sampling which is where we would have found the acrotelm. This is the top most part of the bog that experiences varying water levels, often occurring down to 30-40 cm of depth and usually where the highest accumulation rate is found. The bulk density and PAR are typical for that of a fen with a generally slow decrease as it grows vertically. There is a higher nutrient supply due to a greater input via ground and surface waters during the initial phases of a fen. The bulk density is at its greatest value at the base and similarly decreases PAR until 4390 cal BP. The slight increase from 4390 to 4310 cal BP reflects a shift toward warmer climate conditions while the two rapid decreases between 3840 and 3370 cal BP reflect the transition from nutrient-rich fen to nutrient-poor bog.

The fen-bog transition was mainly identified by the sharp and unique decrease in the ash content from 3840 to 3675 cal BP. The trend of the PAR and the shifts in grain size around this period support the fen-bog division. The PAR initiates with a very short stable period to then decrease rapidly followed by a stable period from 3675 to 2520 cal BP. The nutrient supply in the bog section is initially high and decreases as it receives less minerogenic input when it is cut off from ground and surface waters. Also, suddenly depending solely on aeolian input should lead to a smaller proportion of the coarse material when compared to that of the fen section. The grain size analysis showed a sharp decrease for the median value and also that 100% of the material consisted of the fine size fraction at 3675 cal BP (figure 5).

Svensson (1988) divided the bog into three successive stages with two highly humified layers separating them. One of those stages, the *Rubellum-Fuscum* bog stage, occurred ca. 2400 cal BP and lasted for more than 1000 years. This bog stage is assumed to be reflected by the strong increase in bulk density and PAR from 2520 to 1570 cal BP (figure 4). The two peaks in this stage occur in 2025 and 1735 cal BP. According to Svensson the peat became more humified at ca. 1700 cal BP and this recurrence surface

is found in several bogs across north-western Europe, indicating that the transition is primarily due to a shift in climate. This was likely caused by a shift toward drier and warmer climate conditions. The rapid decrease of the PAR from 1735 to 1570 cal BP, followed by the relatively stable period until 390 cal BP, should reflect a shift toward wetter conditions. Svensson (1988) agrees with this as he describes the transition from the *Rubellum-Fuscum* bog stage to the slightly humified *Magellanicum* bog stage. This transition occurred ca. 1300-1000 cal BP, caused by a strong rise in water table depth.

The difference in timing with Svenssons 2400 and 2520 cal BP recurrence surface from figure 4 can partly be explained by a time offset caused by the poor resolution of the age-depth model (figure 3). Two calibrated age dates is a very low set of values to base a 5200 year old age model on. An abrupt change in gradients for the two linear weighted means is observed at 2828 cal. This is also reflected in the PAR (figure 4) after 2910 cal BP causing a positive shift for the PAR relative to the bulk density until 390 cal BP. Another age-depth model of a 8000 year old peat sequence from Store Mosse looks very different and smoother, similar to a S-curve at the base (Kylander *et al.*, 2013).

## 4.2 Minerogenic sources

Store Mosse has an abundance of local sediment sources, for example glacial sediments like till, glaciofluvial silt and sand as well as sand sheets and dunes (figure 2). These different landforms provide material of different grain sizes to the bog.

The main minerals identified by FTIR-ATR of the peat ash were quartz (Cp1), mica (Cp3) and K-feldspar (Cp5), with quartz dominating. These minerals could indicate that most of the sediments are of local origin since they match with the composition of glacially derived source sediments in the area found by Kylander *et al.* (2023). The four identified minerals could also reflect the bedrock composition since it consists mostly of gneisses and granite. However, gneiss and granite are the most common rocks in Sweden so these minerals could have formed in more than just one place.

The sediment transport rate and deposition of aeolian sediments depends on the wind velocity, grain properties and sediment availability as well as the surrounding environmental conditions such as moisture and vegetation (Vandenberghe, 2013). According to van Rijn (2023), dust particles (<63  $\mu\text{m}$ ) are primarily transported in long-term (<20  $\mu\text{m}$ ) or short-term (20-63  $\mu\text{m}$ ) suspension. The grain size analysis presents a median diameter ( $11,3 \pm 1,9 \mu\text{m}$ ) with an average value below 20  $\mu\text{m}$ . Fine grains like these can be transported in suspension for long distances. van Rijn (2023) also mentions that grains coarser than 100  $\mu\text{m}$  are much more likely to be transported as bed load by saltation, surface creep or reptation. This applies to high energy wind conditions as well. Most of the aeolian transported loads are located within 50 cm of the ground surface. While an increase in wind velocity would generate a higher particle concentration in this thin layer it would also slow down the wind speed near the ground surface. Therefore, this report will assume that only grains coarser than 100  $\mu\text{m}$  are of local origin.

As previously mentioned, sediment transport is also affected by the surrounding environmental conditions. Björckl and Clemmensen (2004) mentions that coarse grains located in the center of the bog have likely been transported by niveo-aeolian processes. The uneven vegetation and moist conditions of the bog prevent the transport of coarser grains by saltation, surface creep or reptation. These bogs are often covered by smooth surfaces of snow and ice during wintertime which facilitates the transport of the coarse grains into the bog.

Bjermo (2019) analyzed the geomorphology of the dunes located in Store Mosse by measuring the steepness of the slopes and identifying the windward side and the lee side to determine the wind pattern that prevailed at the time of their deposition. He concluded that northwesterly wind regimes prevailed at the time of their deposition ca. 8000-6000

cal BP. Unlike the westerly winds that prevail today. Bernhardson *et al.* (2019) conducted a similar type of study over a wider area and reached the same conclusion; northwesterly to westerly winds prevailed in southern Scandinavia during this time. This implies that the SMDN sequence's potential mineral sources are the abundant glaciofluvial sediments located ~1200 m northwest, the dune ridge located ~600 m northwest and the thin layer of till located 200-300 m west (figure 2).

### 4.3 Detecting past storm periods through shifts in grain size

High-energy weather events can be identified in the ombrotrophic section from 3675 to 390 cal BP. The coarse (>125 µm) fraction is used as the primary identifier of storm periods; six smaller and two greater peaks were identified for this size fraction (figure 5). These periods are 3535-3400 (0,8 %), 2980-2955 (1,4 %), 2465-2450 (0,9 %), 2190-2170 (1,1 %), 2005-1900 (4,4 %), 1480-1460 (0,8 %), 1210-1190 (0,3 %), 1005-990 (4,3 %) and 735-715 (0,7 %) cal BP. These are mostly not reflected in the median diameter, except for 2980-2955, 2190-2170 and 1005-990 cal BP. The median instead decreases for the other identified storm periods, partly because one or both of the medium coarse (63-125 µm) and medium (38-125 µm) fractions decrease as well. These two size fractions make up more of the material than the coarse (>125 µm) fraction.

The first main peak for the coarse (>125 µm) fraction is at its maximum value of 4,4 % in 1915-1900 cal BP. Which is a very high value when compared to its average of  $0,8 \pm 1,1$  %. It is also clear from figure 5 that the change is significant. The fine (<38 µm) fraction make up 90 % of the material and the coarse (>125 µm) fraction make up a little less than 5 % in the remaining 10 %. While the sharp increase for the coarse (>125 µm) fraction isn't reflected in the median, which displays low values from 2010 to 1845 cal BP, it instead reflects the decrease for medium coarse (63-125 µm) and medium (38-63 µm) fractions. The second main peak for the coarse (>125 µm) fraction in 1005-990 cal BP also involves a decrease for the medium coarse (63-125 µm) and medium (38-63 µm) fractions, but not as much as for the first main peak in 1915-1900 cal BP. Also, the fine (<38 µm) fraction has its lowest value here (82,8 %) and the three largest size fractions make up about 17 % of the material and therefore generate a higher median diameter value of 14,6 µm.

The changes in median diameter don't correspond well to the changes in the coarse (>125 µm) fraction as this fraction makes up so little of the material. While the median diameter can still be used to indicate high-energy events, it should not be used as a single proxy reconstruction. The changes in distribution are important and coarse mineral grains with a diameter of at least 100 µm should be included.

Determining the intensity of paleo-storms through a grain size analysis alone is difficult. Numerous studies have tried to link wind velocities to different grain sizes, often with contradicting results (Van Hateren *et al.*, 2019; van Rijn, 2023). Researchers often put forward models that reflect ideal conditions, for example, like a horizontal surface with no vegetation or uniform composition of particles. Yang *et al.* (2019) models show exponential relationships between mean grain sizes and wind velocities. However, a clear correspondence between grain sizes and different wind velocities would not be sufficient here. We can't know the original particle-size prior to deposition since the sediments have been exposed to aeolian weathering and the acidic environment of the bog. Therefore, storm intensity is not measured directly in terms of wind speed but rather by looking into trends and relative changes.

#### 4.4 Comparing shifts in grain size and mineral composition

Potential source sediments in and around Store Mosse were analyzed for mineral composition (FTIR-ATR) and grain size by Kylander *et al.* (2023). Their results indicated a strong link between quartz (Cp1) and coarser (>63  $\mu\text{m}$ ) grain sizes and also between mica (Cp3) and fine (<38  $\mu\text{m}$ ) grain sizes. K-feldspar (Cp5) was used as an indicator of increased mineral input, it did not show a strong link to a certain size fraction like quartz (Cp1) or mica (Cp3). In this work, sharp increases and “event-like” changes in the relative changes in quartz (Cp1) are used to identify stormier events or periods. The quartz (Cp1) profile in the ombrotrophic section has its peaks centered on 3675, 3535-3400, 3095, 2685, 2355, 2170, 2080-1990, 1480-1425, 825-805, 645 and 460 cal BP (figure 6).

A comparison between the quartz-based storm events with those identified using the coarse (>125  $\mu\text{m}$ ) fraction (3565-3400, 2980-2950, 2465-2450, 2190-2170, 2005-1900, 1480-1460, 1210-1190, 1005-990 and 735-715 cal BP) shows that only four periods are related. Those are dated to 3565-3400, 2190-2170, 2005-1900 and 1480-1460 cal BP. Only a few of the peaks for quartz are sharp though, for example 1480-1425 cal BP displays the maximum values but the sharp increase occurs before from 1915 to 1660 cal BP and most of the changes are gradual until 1005 cal BP.

K-feldspar (Cp5) only displays two peaks which agree with the storm events identified in the coarse (>125  $\mu\text{m}$ ) fraction. Those are 2190-2170 and 1005-990, cal BP. It should be noted that most peaks for K-feldspar (Cp5) don't match with the identified storm periods from the grain size analysis. Mica (Cp3) displays four peaks which match with the storm events identified in the grain size analysis. Those are: 3565-3400, 2980-2950, 1210-1190, 1005-990 and 735-715 cal BP. Nonetheless, since mica belongs to the fine size fraction and K-feldspar can't be linked to any, they will not be used to identify any new storms related to the coarse (>125  $\mu\text{m}$ ) fraction.

The two storms deemed to be most severe based on the distribution of the coarse (>125  $\mu\text{m}$ ) fraction were in 2005-1900 and 1005-990 cal BP and they are not reflected very well in the changes of the mineral composition. Quartz (Cp1), mica (Cp3) and K-feldspar (Cp5) decrease between 1990 and 1900 cal BP while mica (Cp3) and K-feldspar (Cp5) increase only slightly in 1005-990 cal BP. Another interesting observation is the peak in 3675 cal BP for both quartz (Cp1) and K-feldspar (Cp3). This is the fen-bog transition where the ash content decreased rapidly and the grain size analysis showed that 100 % of the material are within the fine (<38  $\mu\text{m}$ ) fraction.

These comparisons indicate that the relationship between grain size distribution and mineral composition is complex. It is difficult to know which method is more trustworthy. The sharp peak displayed for quartz in 3675 cal BP, despite 100 % of the material belonging to the fine (<38  $\mu\text{m}$ ) fraction, proves that increases in quartz (Cp1) only indicates a higher probability of coarse sediments but they could be fine grained. On the other hand, the grain size analysis has a poorer resolution than the FTIR-ATR data. Since two adjacent samples had to be measured together from 3425 to 445 cal BP due to the low mineral content which caused low obscuration values that were commonly below 2%. Measuring two samples together impacts the data since, for example, a sample containing coarse grains would be diluted with one containing more of the fine size fraction. This shows the importance of applying and matching different proxy reconstructions to the same sequence. Four storm periods remain when combining both the quartz-based proxy with those identified using the coarse (>125  $\mu\text{m}$ ) fraction. These are dated to 3565-3400, 2190-2170, 2005-1900 and 1480-1460 cal BP.

## 4.5 SMDN storm record compared to SMDS storm record

The SMDS storm record was made by Kylander *et al.* (2023) based on past changes in mineral composition by FTIR-ATR supported by elemental variations measured with XRF core scanning (XRF-CS) (figure 7 and 8). The SMDS sequence has a basal age of 4755 cal BP while the SMDN sequence basal age dates to approximately 5300 cal BP. Bulk density, PAR and ash content values are lower for the SMDS record ( $0,07 \pm 0,02 \text{ g cm}^{-3}$ ,  $60 \pm 19 \text{ g m}^{-2} \text{ yr}^{-1}$ ,  $1,0 \pm 0,2\%$ ) compared to the SMDN record ( $0,12 \pm 0,06 \text{ g cm}^{-3}$ ,  $109 \pm 47 \text{ g m}^{-2} \text{ yr}^{-1}$ ,  $1,6 \pm 1,3 \%$ ). The transition from minerotrophic fen to ombrotrophic bog occurred at ca. 4100 cal BP and the peat ash is mainly made up of quartz, mica, K-feldspar and Ca-feldspar. The mineral sources are assumed to primarily be the sand dunes located ~1 km northwest of SMDS (figure 2). Paleo-storms were identified through higher ratios of quartz and Si/Al which indicates the presence of coarse material, while K-feldspar and mica were used as indicators of increased mineral input. The SMDS record estimated seven storm periods dated to 4480-4425, 3320-3190, 2150-1920, 1450, 1005-850, 720-650 and 410-350 cal BP.

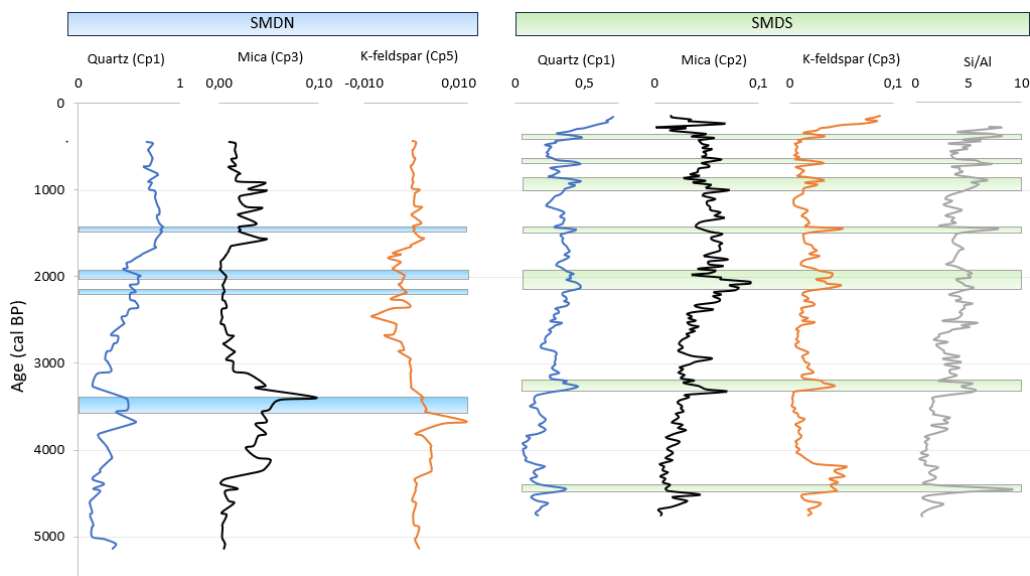


Figure 7. Relative changes in mineral composition for the SMDN and SMDS record and also elemental variations (Si/Al) for the SMDS record. The colored boxes represent identified storm periods in each record. SMDN: 3565-3400, 2190-2170, 2005-1900 and 1480-1460 cal BP. SMDS: 4480-4425, 3320-3190, 2150-1920, 1450, 1005-850, 720-650 and 410-350 cal BP.

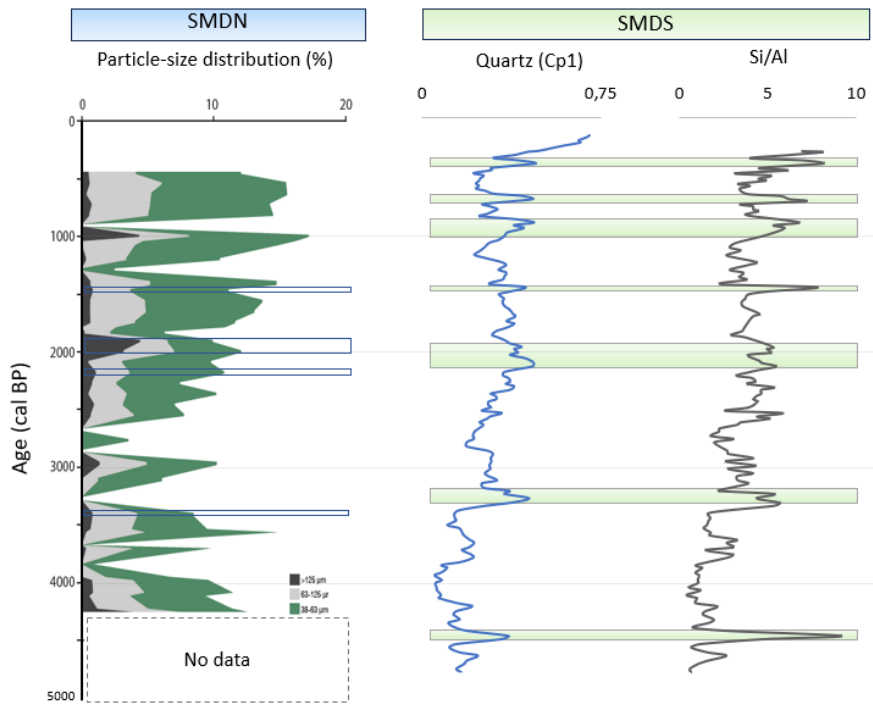


Figure 8. Grain size distribution profile for the SMDN record and the relative changes in mineral composition and elemental variations for the SMDS record. The grain size distribution is divided into three size fractions: coarse ( $>125 \mu\text{m}$ ), medium coarse ( $63\text{-}125 \mu\text{m}$ ) and medium ( $38\text{-}63 \mu\text{m}$ ). The fine ( $<38 \mu\text{m}$ ) fraction is not presented in the figure but makes up the remainder of the material through the profile. The boxes represent identified storm periods in each storm record. SMDN: 3565-3400, 2190-2170, 2005-1990 and 1480-1460 cal BP. SMDS: 4480-4425, 3320-3190, 2150-1920, 1450, 1005-850, 720-650 and 410-350 cal BP.

A comparison of identified storm periods between the SMDN and SMDS record found three to be related, when taking the time offset into consideration caused by the difference in number of measured and calibrated  $^{14}\text{C}$  dates (figure 7 and 8). The three storm periods from the SMDN record which agree with the SMDS record, or rather are close in time to, are dated to 2190-2170 (SMDS: 2150-1920 cal BP), 2005-1990 (SMDS: 2150-1920) and 1480-1425 (SMDS: 1450 cal BP) cal BP. Two of the storm periods in SMDN overlap with 2150-1920 cal BP from SMDS. The storm period 3565-3400 cal BP differs more in time from 3320-3190 cal BP recorded in SMDS than the other identified storms and is therefore not included.

The storm periods dated from the SMDS record which could not be identified in the SMDN record were 4480-4425, 3320-3190, 1005-850, 720-650 and 410-350 cal BP. The fen-bog transition occurred earlier in the SMDS record which is why the storm period dated to 4480-4425 cal BP is not included in SMDN. The grain size and FTIR-ATR analysis starts at 445 cal BP, the storm period 410-350 cal BP is therefore not part of the SMDN record. Still, the SMDS record identified more storm periods between 3675 and 445 cal BP. Several different factors could have affected this.

Reconstructing past storm events by combining grain size distribution analysis with changes in mineral composition might not be a good method or maybe it should be applied differently. As stated previously, the comparisons between grain-size distribution and changes in mineral composition indicated that the relationship between these two is complex. Nine potential storm events were identified in the quartz-based proxy record and eleven using the coarse ( $>125 \mu\text{m}$ ) fraction, only four remained after a comparison between these two (figure 7 and 8). The peaks used to identify storm events in quartz were not very sharp though. Also, two more storm periods related to the identified storms from SMDS can be identified by peaks in the coarse ( $>125 \mu\text{m}$ ) fraction

alone (figure 8), those are 1005-990 (SMDS: 1005-850 cal BP) and 735-715 (SMDS: 720-650 cal BP) cal BP. Another approach could be to define the peaks from each proxy reconstruction in wide intervals as they might not occur simultaneously. The lack of agreement between SMDS and SMDN could also be related to site.

Another explanation could be that the conditions of the bog affect the storm signal. Storm periods dated to 3565-3400 cal BP (SMDN) and 3320-3190 (SMDS) cal BP are located further down in the records which might affect both grain size and mineral composition since they have been subjected to the acidic bog environment for a longer period of time. This doesn't explain the lack of agreement for storm periods dated to 1005-850 and 720-650 cal BP though.

Kylander *et al.* (2023) compared their reconstructed SMDS storm record to the Store Mosse South-2008 sequence collected from the southern parts of Store Mosse, below Blådöpet. Although the sequences shared many recorded storm events/periods, they also found differences early in the record. They suggested shifts in dominant wind directions to be the cause for this as it could potentially affect distances between mineral source and sample location.

There has to be an abundance of sediment sources located downwind and close to the bog for a storm signal to be recorded. As mentioned previously, according to Bjermo (2019) and Bernhardson *et al.* (2019) it is likely that northwesterly to westerly winds prevailed ca. 8000-6000 cal BP, unlike the westerly winds today. When examining the soil map (figure 2), it may seem counterintuitive at first that SMDS would have more storm events recorded. Since the mineral sources northwest of SMDN are located closer than those of SMDS, and consists of glaciofluvial silt/sand, till and sand dunes/sheets. Although the till is only a thin layer and may contain grains too coarse for transport, these different landforms should contain more coarse grains than the dunes located ~1 km northwest of SMDS.

While the progression toward westerly winds might initially decrease the transport distance between the mineral source and SMDN, generating a stronger storm signal. It may eventually lead to a longer transport distance as the potential mineral source would change to glaciofluvial sand located ~2,5 km west of SMDN (figure 2). Winds from this direction would have to be stronger to transport and generate a storm signal, which risks creating a gap in the record. Considering this, it would imply that SMDS is not as vulnerable to changing wind directions as it has more storm events recorded. The dunes separating SMDN and SMDS extend over a wider area, almost perpendicular to the prevailing wind conditions of the last 8000-6000 years. This indicates that material can be provided more continuously to this part of the bog, which could make SMDS a more reliable proxy record while also explaining the lack of agreement between SMDN and SMDS. This shows the importance of analyzing different sequences within the same site.

## 4.6 Conclusions

The aim of this project was to reconstruct the paleo-storm record in the SMDN sequence over the last 5200 years and to compare it to the SMDS storm record made by Kylander *et al.* (2023). A peat profile was created to distinguish between the minerotrophic fen and ombrotrophic bog, the fen initiated 5170 cal BP and became fully ombrotrophic in 3675 cal BP.

Grain size analysis and changes in mineral composition measured by FTIR-ATR were used individually to identify storm periods. The results showed that the fine (<38  $\mu\text{m}$ ) fraction dominates the signal and the main minerals identified were quartz (Cp1), mica (Cp3) and K-feldspar (Cp5). Nine potential storm periods were identified through peaks in the coarse (>125  $\mu\text{m}$ ) size fraction and eleven in quartz (Cp1). A comparison between these two left four storm periods/events, these are dated to 3565-3400, 2190-

2170, 2005-1900 and 1480-1460 cal BP. This shows the importance of using and applying different proxy reconstructions.

Three storm periods, between 3675 and 390 cal BP, from the SMDN storm record matched with the SMDS storm record. These were 2190-2170 (SMDS: 2150-1920 cal BP), 2005-1990 (SMDS: 2150-1920) and 1480-1425 (SMDS: 1450 cal BP) cal BP. Several different factors could have caused this. The main cause is believed to be shifting wind directions, where northwesterly winds would supply SMDN with more coarse material but a progression toward westerly wind directions would cause a shift in mineral source and increased transport length. Thus, weakening the storm signal. This shows the importance of analyzing different sequences within the same site.

## Acknowledgement

I would like to sincerely thank my supervisor Dr Malin Kylander for giving me this opportunity and for the invaluable support. Providing me with articles on the subject, data and insightful comments.

I would also like to thank Dr Carina Johansson and Dr Jenny Sjöström for their help in the lab. I also want to express my gratitude to Megan Windell for her patience, support and very thorough instructions in the lab.

Lastly, I want to thank my mum, my brother and his girlfriend Emelie who offered joy, encouragement and made the trip to Store Mosse possible.

## References

- Arias, P.A., N. Bellouin, E. Coppola, R.G. Jones, G. Krinner, J. Marotzke, V. Naik, M.D. Palmer, G.-K. Plattner, J. Rogelj, M. Rojas, J. Sillmann, T. Storelvmo, P.W. Thorne, B. Trewin, K. Achuta Rao, B. Adhikary, R.P. Allan, K. Armour, G. Bala, R. Barimalala, S. Berger, J.G. Canadell, C. Cassou, A. Cherchi, W. Collins, W.D. Collins, S.L. Connors, S. Corti, F. Cruz, F.J. Dentener, C. Dereczynski, A. Di Luca, A. Diongue Niang, F.J. Doblas-Reyes, A. Dosio, H. Douville, F. Engelbrecht, V. Eyring, E. Fischer, P. Forster, B. Fox-Kemper, J.S. Fuglestedt, J.C. Fyfe, N.P. Gillett, L. Goldfarb, I. Gorodetskaya, J.M. Gutierrez, R. Hamdi, E. Hawkins, H.T. Hewitt, P. Hope, A.S. Islam, C. Jones, D.S. Kaufman, R.E. Kopp, Y. Kosaka, J. Kossin, S. Krakovska, J.-Y. Lee, J. Li, T. Mauritsen, T.K. Maycock, M. Meinshausen, S.-K. Min, P.M.S. Monteiro, T. Ngo-Duc, F. Otto, I. Pinto, A. Pirani, K. Raghavan, R. Ranasinghe, A.C. Ruane, L. Ruiz, J.-B. Sallée, B.H. Samset, S. Sathyendranath, S.I. Seneviratne, A.A. Sörensson, S. Szopa, I. Takayabu, A.-M. Tréguier, B. van den Hurk, R. Vautard, K. von Schuckmann, S. Zaehle, X. Zhang, and K. Zickfeld, 2021: Technical Summary. In *Climate Change 2021: The Physical Science Basis. Contribution of Working Group I to the Sixth Assessment Report of the Intergovernmental Panel on Climate Change* [Masson-Delmotte, V., P. Zhai, A. Pirani, S.L. Connors, C. Péan, S. Berger, N. Caud, Y. Chen, L. Goldfarb, M.I. Gomis, M. Huang, K. Leitzell, E. Lonnoy, J.B.R. Matthews, T.K. Maycock, T. Waterfield, O. Yelekçi, R. Yu, and B. Zhou (eds.)]. Cambridge University Press, Cambridge, United Kingdom and New York, NY, USA, pp. 33–144. doi:10.1017/9781009157896.002
- Adamsson, L. (2013) Peat stratigraphical study of hydrological conditions at Stass Mosse, southern Sweden, and the relation to Holocene bog-pine growth. Master's thesis. Dissertations in Geology, Lund University. Available at: <http://lup.lub.lu.se/student-papers/record/3807020> (Accessed: 21 May 2024).
- Bannister, D. et al. (2024) European Windstorms: The Role of the North Atlantic Oscillation in Estimating Return Levels, WTW. Available at: <https://www.wtwco.com/en-vn/insights/2024/01/european-windstorms-the-role-of-the-north-atlantic-oscillation-in-estimating-return-levels> (Accessed: 20 May 2024).
- Belyea, L.R. and Malmer, N. (2004) 'Carbon sequestration in peatland: patterns and mechanisms of response to climate change', *Global Change Biology*, 10(7), pp. 1043–1052. Available at: <https://doi.org/10.1111/j.1529-8817.2003.00783.x>.
- Bernhardson, M. et al. (2019) 'Sand drift events and surface winds in south-central Sweden: From the deglaciation to the present', *Quaternary Science Reviews*, 209, pp. 13–22. Available at: <https://doi.org/10.1016/j.quascirev.2019.01.017>.
- Bjermo, T. (2019) Eoliska avlagringar och vindriktningar under holocen i och kring Store Mosse, södra Sverige. Bachelor thesis. Lund, Sweden: Geological Department, Lund University, p. 62. Available at: <https://lup.lub.lu.se/luur/download?func=downloadFile&recordId=8983090&fileId=8983202> (Accessed: 22 May 2024).
- Björckl, S. and Clemmensen, L.B. (2004) 'Aeolian sediment in raised bog deposits, Halland, SW Sweden: a new proxy record of Holocene winter storminess

- variation in southern Scandinavia?', *The Holocene*, 14(5), pp. 677–688. Available at: <https://doi.org/10.1191/0959683604hl746rp>.
- Chambers, F.M. et al. (2012) 'Development and refinement of proxy-climate indicators from peats', *Quaternary International*, 268, pp. 21–33. Available at: <https://doi.org/10.1016/j.quaint.2011.04.039>.
- Fernandez, N.A. and Cortizas, A.M. (2020) 'andurinha: Make Spectroscopic Data Processing Easier'. Available at: <https://cran.r-project.org/web/packages/andurinha/index.html> (Accessed: 26 May 2024).
- Franzén, L.G. (2006) 'Chapter 11 Mineral matter, major elements, and trace elements in raised bog peat: a case study from southern Sweden, Ireland and Tierra del Fuego, south Argentina', in I.P. Martini, A. Martínez Cortizas, and W. Chesworth (eds) *Developments in Earth Surface Processes*. Elsevier (Peatlands), pp. 241–269. Available at: [https://doi.org/10.1016/S0928-2025\(06\)09011-0](https://doi.org/10.1016/S0928-2025(06)09011-0).
- Hansson, A. (2013) 'A dendroclimatic study at Store Mosse, South Sweden : climatic and hydrologic impacts on recent Scots Pine (*Pinus sylvestris*) growth dynamics', *Dissertations in Geology at Lund University*, p. 34.
- IPCC (2021) *Climate Change 2021 – The Physical Science Basis: Working Group I Contribution to the Sixth Assessment Report of the Intergovernmental Panel on Climate Change*. 1st edn. Cambridge University Press. Available at: <https://doi.org/10.1017/9781009157896>.
- de Jong, R. (2007) *Stormy records from peat bogs in south-west Sweden : implications for regional climatic variability and vegetation changes during the past 6500 years*. Doctoral thesis (compilation), Quaternary Sciences. Department of geology, Lund University. Available at: <https://lucris.lub.lu.se/ws/portalfiles/portal/4603591/3163688.pdf> (Accessed: 6 May 2024).
- Kylander, M.E. et al. (2013) 'A novel geochemical approach to paleorecords of dust deposition and effective humidity: 8500 years of peat accumulation at Store Mosse (the "Great Bog"), Sweden', *Quaternary Science Reviews*, 69, pp. 69–82. Available at: <https://doi.org/10.1016/j.quascirev.2013.02.010>.
- Kylander, M.E. et al. (2023) 'Storm chasing: Tracking Holocene storminess in southern Sweden using mineral proxies from inland and coastal peat bogs', *Quaternary Science Reviews*, 299, p. 107854. Available at: <https://doi.org/10.1016/j.quascirev.2022.107854>.
- Lachance, A. (2022) *Peatlands to the Rescue! Late Holocene History of Climate and Storms as Told by Coastal Peatlands on the Magdalen Islands, Québec, Canada*. Master of Science. Concordia University. Available at: [https://spectrum.library.concordia.ca/id/eprint/991372/1/Lachance\\_MSc\\_S2023.pdf](https://spectrum.library.concordia.ca/id/eprint/991372/1/Lachance_MSc_S2023.pdf) (Accessed: 1 May 2024).
- Lachance, A., Peros, M. and St-Jacques, J.-M. (2022) *Peatbogs to the rescue! Opportunities and challenges in using ombrotrophic peat cores for a reconstruction of paleo-storms during the Holocene in eastern Canada*. EGU22-10953. Copernicus Meetings. Available at: <https://doi.org/10.5194/egusphere-egu22-10953>.

- Lundqvist, J. and Wohlfarth, B. (2001) 'Timing and east–west correlation of south Swedish ice marginal lines during the Late Weichselian', *Quaternary Science Reviews*, 20(10), pp. 1127–1148. Available at: [https://doi.org/10.1016/S0277-3791\(00\)00142-6](https://doi.org/10.1016/S0277-3791(00)00142-6).
- Martínez-Cortizas, A. et al. (2021) 'Investigating the Mineral Composition of Peat by Combining FTIR-ATR and Multivariate Analysis', *Minerals* 2021, 11, 1084, p. 15. Available at: <https://doi.org/10.3390/min11101084>.
- Nielsen, P.R. et al. (2024) 'Intensified Late-Holocene aeolian activity in Vesterålen, northern Norway – increased storminess or human impact?', *The Holocene*, 34(5), pp. 554–567. Available at: <https://doi.org/10.1177/09596836231225724>.
- Orme, L.C. (2014) Reconstructions of Late Holocene storminess in Europe and the role of the North Atlantic Oscillation. Thesis degree of Doctor of Philosophy in Geography. University of Exeter. Available at: <https://ore.exeter.ac.uk/repository/bitstream/handle/10871/16128/OrmeL.pdf?sequence=4> (Accessed: 3 May 2024).
- Persson, M. (2008) 'Beskrivning till jordartskartan 5D Värnamo NO', Sveriges geologiska undersökning, SGU, (K113), p. 12.
- van Ravenhorst, L. (2022) Peatland restoration: A mossy affair? The similarities of the vegetation communities between restored bogs and natural bogs. Master of Science, biology. Uppsala University. Available at: <https://uu.diva-portal.org/smash/get/diva2:1722133/FULLTEXT01.pdf>.
- Reimer, P.J. et al. (2020) 'The IntCal20 Northern Hemisphere Radiocarbon Age Calibration Curve (0–55 cal kBP)', *Radiocarbon*, 62(4), pp. 725–757. Available at: <https://doi.org/10.1017/RDC.2020.41>.
- van Rijn, L.C. (2023) 'Aeolian sand transport processes, Part 1: model formulation and calibration'. Available at: <https://www.leovanrijn-sediment.com/papers/Aeoliansandtransport2018.pdf> (Accessed: 23 May 2024).
- Ryberg, E.E. et al. (2022) 'Postglacial peatland vegetation succession in Store Mosse bog, south-central Sweden: An exploration of factors driving species change', *Boreas* 51, pp. 651–666. Available at: <https://doi.org/10.1111/bor.12580>.
- Rydin, H. and Jeglum, J.K. (2013a) *The Biology of Peatlands*. Oxford University Press. Available at: <https://doi.org/10.1093/acprof:osobl/9780199602995.001.0001>.
- Rydin, H. and Jeglum, J.K. (2013b) 'The peat archives', in H. Rydin and J.K. Jeglum (eds) *The Biology of Peatlands*. Oxford University Press, p. 0. Available at: <https://doi.org/10.1093/acprof:osobl/9780199602995.003.0006>.
- Schwierz, C. et al. (2010) 'Modelling European winter wind storm losses in current and future climate', *Climatic Change*, 101(3), pp. 485–514. Available at: <https://doi.org/10.1007/s10584-009-9712-1>.
- Severino, L.G. et al. (2024) 'Projections and uncertainties of winter windstorm damage in Europe in a changing climate', *Natural Hazards and Earth System Sciences*, 24(5), pp. 1555–1578. Available at: <https://doi.org/10.5194/nhess-24-1555-2024>.
- SGU (2018) SGUs Kartvisare, Sveriges geologiska undersökning. Available at: <https://apps.sgu.se/kartvisare/kartvisare-jordarter-25-100.html> (Accessed: 22 May 2024).

Sjöström, J.K. et al. (2022) 'Late Holocene peat paleodust deposition in south-western Sweden - exploring geochemical properties, local mineral sources and regional aeolian activity', *Chemical Geology*, 602, p. 120881. Available at: <https://doi.org/10.1016/j.chemgeo.2022.120881>.

SMHI (2023) Skalar för vindhastighet, SMHI. Available at: <https://www.smhi.se/kunskapsbanken/meteorologi/vind/skalar-for-vindhastighet-1.252> (Accessed: 25 May 2024).

SMHI (2024a) Ladda ner meteorologiska observationer | Lufttemperatur, SMHI. Available at: <https://www.smhi.se/data/meteorologi/ladda-ner-meteorologiska-observationer/#param=airtemperatureInstant,stations=core,stationid=74180> (Accessed: 21 May 2024).

SMHI (2024b) Ladda ner meteorologiska observationer | Nederbördsmängd, SMHI. Available at: <https://www.smhi.se/data/meteorologi/ladda-ner-meteorologiska-observationer/#param=precipitationHourlySum,stations=core,stationid=74180> (Accessed: 21 May 2024).

Sohlenius, G. et al. (2013) 'Development, carbon balance and agricultural use of peatlands – overview and examples from Uppland Sweden', SKB, p. 79.

Svensson, G. (1988) 'Bog development and environmental conditions as shown by the stratigraphy of Store Mosse mire in southern Sweden', *Boreas*, 17(1), pp. 89–111. Available at: <https://doi.org/10.1111/j.1502-3885.1988.tb00126.x>.

Sveriges Nationalparker (2024) Geologi - Store Mosse nationalpark, Sveriges Nationalparker. Available at: <https://www.sverigesnationalparker.se/park/store-mosse-nationalpark/nationalparksfakta/geologi/> (Accessed: 21 May 2024).

Van Hateren, J.A. et al. (2019) 'Identifying sediment transport mechanisms from grain size-shape distributions'. Available at: <https://doi.org/10.5194/esurf-2019-58>.

Vandenbergh, J. (2013) 'Grain size of fine-grained windblown sediment: A powerful proxy for process identification', *Earth-Science Reviews*, 121, pp. 18–30. Available at: <https://doi.org/10.1016/j.earscirev.2013.03.001>.

Vikdahl, O. (2021) Reconstruction of past atmospheric mineral dust over the last 5200 cal yr BP using geochemical proxies from Store Mosse, Sweden. Bachelor thesis. Stockholm University. Available at: [https://www.su.se/polopoly\\_fs/1.559847.1623138177!/menu/standard/file/2021\\_Oskar-Vikdahl\\_BSc-Geoscience\\_15hp.pdf](https://www.su.se/polopoly_fs/1.559847.1623138177!/menu/standard/file/2021_Oskar-Vikdahl_BSc-Geoscience_15hp.pdf) (Accessed: 29 April 2024).

Yang, Y. et al. (2019) 'Aerodynamic grain-size distribution of blown sand', *Sedimentology*, 66(2), pp. 590–603. Available at: <https://doi.org/10.1111/sed.12497>.

Yao, Q. et al. (2023) 'What Are the Most Effective Proxies in Identifying Storm-Surge Deposits in Paleotempestology? A Quantitative Evaluation From the Sand-Limited, Peat-Dominated Environment of the Florida Coastal Everglades', *Geochemistry, Geophysics, Geosystems*, 24(3), p. e2022GC010708. Available at: <https://doi.org/10.1029/2022GC010708>.

## Appendix

### Appendix A: Pre-treated mineral content from Cores 1 and 6



Photo displaying the differences in the amount of mineral content in core 6 (left) and core 1 (right). The material for core 1 is after being vortexed for 10 seconds prior to measurement in the Malvern 3000 laser diffraction particle size analyzer.